

Supporting Information for

Regular Double-Cube $[\text{Cr}_7\text{S}_8]^{5+}$ in $[\text{Cr}_7\text{S}_8(\text{SCN})_4(\text{NH}_3)_{14}](\text{HS})$: An Ideal Model Compound for Investigation of Geometrical Magnetic Frustration

Jia Yang,^{†,‡} Pengfei Jiang,^{*,†,§} Zhengyang Zhou,[#] Mufei Yue,[†] Dingfeng Yang,[†] Shijian Chen,[§] Tao Yang^{*,†}

[†]College of Chemistry and Chemical Engineering, Chongqing University, Chongqing 401331, P. R. China.

[‡]School of Chemistry and Chemical Engineering, Yangtze Normal University, Chongqing 408100, P. R. China.

[§]College of physics, Chongqing University, Chongqing 401331, P. R. China.

[#]College of Chemistry and Molecular Engineering, Peking University, Beijing 100871, P. R. China.

*E-mails: pengfeijiang@cqu.edu.cn; taoyang@cqu.edu.cn.

SI Characterization

Single-crystal XRD data were collected on an Agilent Technologies SuperNova Dual Wavelength CCD diffractometer with Mo K α radiation ($\lambda = 0.71073 \text{ \AA}$) at 293 K. The crystal structure was solved by direct method in space group $P4_2/m$ and refined by full-matrix least-squares fitting on F^2 using SHELX-97. Crystallographic data and structure refinement are summarized in Table S1. Atomic coordinates, occupancies, and isotropic thermal factors are list in Table S2. Selected interatomic distances and bond angles are list in Table S3.

Powder X-ray diffraction data for $[\text{Cr}_7\text{S}_8(\text{SCN})_4(\text{NH}_3)_{14}](\text{SH})$ was collected on the PANalytic X'pert diffractometer with Cu K α radiation. The operation voltage and current were 40 kV and 40 mA, respectively. The XRD data were collected with the setting of 0.0262/20s. The specific surface areas for $\text{Cr}_2\text{S}_{3-x}\text{O}_x$ were estimated according to the Brunauer-Emmertt-Teller (BET) method with N_2 adsorption-desorption isothermals at 77 K using a Quantachrome Quadrasorb SI analyzer. Scanning electron microscopies (SEM) were performed on JSM-7800F electron microscope with an accelerating voltage of 3.0 kV. The thermal decomposition process for $[\text{Cr}_7\text{S}_8(\text{SCN})_4(\text{NH}_3)_{14}](\text{SH})$ was assessed by thermogravimetric analysis (TGA) and differential scanning calorimetry (DSC) method using Shimadzu DTG-60h with heating rate of 5 $^\circ\text{C}/\text{min}$ in air from room temperature to 800 $^\circ\text{C}$. The magnetic data were collected on a Quantum Design DynaCool system.

Table S1 Crystallographic data for $[\text{Cr}_7\text{S}_8(\text{SCN})_4(\text{NH}_3)_{14}](\text{SH})$.

Empirical formula	$[\text{Cr}_7\text{S}_8(\text{SCN})_4(\text{NH}_3)_{14}](\text{SH})$
Mr (g/mol)	2248.68
Space group (number)	$P4_2/m$ (84)
Lattice parameters (Å)	$a = 11.3608(3)$, $c = 16.2437(7)$
Cell volume (Å ³)	2095.39(14)
Z	1
Density (g/cm ³)	1.782
Temperature (K)	293(2)
μ (Mo K α), mm ⁻¹	2.425
F(000)	1138
Refinement method	Full-matrix least squares on F^2
Final R1	0.0354
wR ₂ [$I > 2\sigma(I)$]	0.0875
GoF	1.052

Table S2. Atomic coordinates, occupancy factors and isotropic thermal displacement parameters for $[\text{Cr}_7\text{S}_8(\text{SCN})_4(\text{NH}_3)_{14}](\text{SH})$.

Atom	x	y	z	Occ.	$U_{\text{iso.}}$ (Å ²)
Cr1	0.500	0.500	0	1	0.0118(2)
Cr2	0.24034(4)	0.46830(5)	-0.10356(3)	1	0.0142(2)
Cr3	0.29383(7)	0.71860(7)	0	1	0.0164(2)

S1	0.33918(1)	0.36182(1)	0	1	0.0140(3)
S2	0.14028(1)	0.57745(9)	0	1	0.0150(3)
S3	0.39319(8)	0.61078(8)	-0.10278(4)	1	0.0150(2)
S4a	0.3305(2)	1.0602(1)	-0.1666(1)	0.880(5)	0.0574(6)
S4b	0.2702(15)	1.059(1)	-0.204(1)	0.120(5)	0.0574(6)
S5	0.0624(5)	0.0651(5)	0	0.5	0.070(2)
N1	0.1059(3)	0.3399(3)	0.1097(2)	1	0.0221(7)
N2	0.2016(3)	0.8134(3)	-0.0924(2)	1	0.0311(7)
N3	0.4307(4)	0.8456(4)	0	1	0.0252(9)
N4	0.3326(3)	0.3688(3)	-0.18984(18)	1	0.0199(6)
N5	0.1516(2)	0.5526(2)	-0.1969(2)	1	0.0223(6)
C1	0.1106(3)	0.5992(4)	-0.2527(2)	1	0.0318(8)

Table S3 Selected bond distances (Å) and angles (°) for $[\text{Cr}_7\text{S}_8(\text{SCN})_4(\text{NH}_3)_{14}](\text{SH})$.

Bonds/bond angles	Length/degree	Bonds/bond Angles	Length/degree
Cr1-S1	2.409(1)	Cr2-N4	2.083(3)
Cr1-S3	2.4177(7)	Cr2-N5	2.056(3)
Cr2-S1	2.3561(8)	Cr3-S2	2.3695(12)
Cr2-S2	2.3783(9)	Cr3-S3	2.3587(9)
Cr2-S3	2.3740(8)	Cr3-N2	2.123(3)
Cr2-N1	2.115(3)	Cr3-N3	2.121(4)
N5-C1	1.148(4)	S4a-C1	1.639(4)

S4b-C1	1.745(13)		
S1-Cr1-S1	180	N4-Cr2-N1	87.59(12)
S1-Cr1-S3	92.37(2)	N5-Cr2-S1	176.86(8)
S1-Cr1-S3	87.63(2)	N5-Cr2-S2	92.50(8)
S3-Cr1-S3	87.38(3)	N5-Cr2-N1	86.12(12)
S3-Cr1-S3	92.62(4)	N5-Cr2-N4	90.23(12)
S3-Cr1-S3	87.38(4)	S3-Cr3-S2	90.05(3)
S3-Cr1-S3	180	S3-Cr3-S3	90.15(4)
S1-Cr2-S2	89.49(3)	N2-Cr3-S2	88.86(8)
S1-Cr2-S3	89.89(3)	N2-Cr3-S3	178.90(9)
S3-Cr2-S2	89.47(3)	N2-Cr3-S3	89.97(9)
N1-Cr2-S1	91.35(9)	N2-Cr3-N2	89.9(2)
N1-Cr2-S2	92.72(9)	N3-Cr3-S2	179.74(13)
N1-Cr2-S3	177.49(9)	N3-Cr3-S3	90.13(9)
N4-Cr2-S1	87.79(9)	N3-Cr3-N2	90.96(12)
N4-Cr2-S2	177.27(9)	C1-N5-Cr2	174.3(3)
N4-Cr2-S3	90.28(9)		



Figure S1. Photographs for single crystals of $[\text{Cr}_7\text{S}_8(\text{SCN})_4(\text{NH}_3)_{14}](\text{SH})$ (~ 0.5 mm in length).

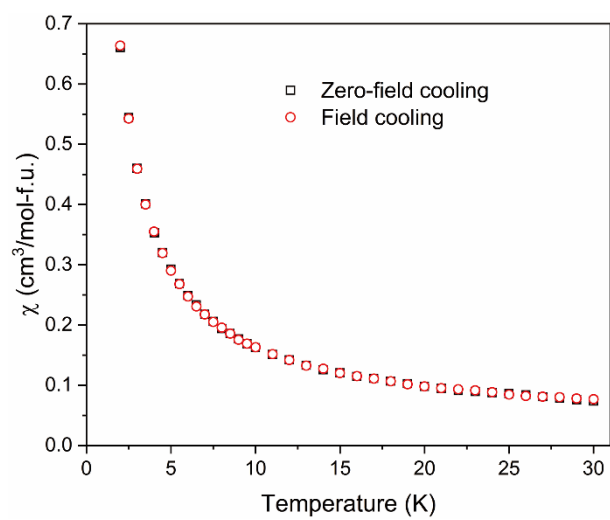


Figure S2. Temperature dependent zero-field-cooling and field-cooling magnetic susceptibilities measured under an external field of 50 Oe.

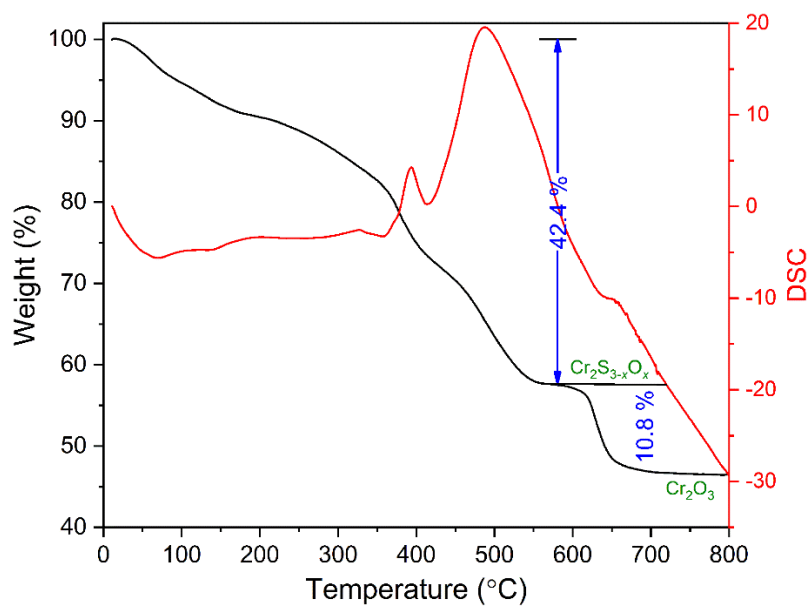


Figure S3. The TGA and DSC curves for $[\text{Cr}_7\text{S}_8(\text{SCN})_4(\text{NH}_3)_{14}](\text{SH})$ measured in the temperature range of room temperature to 800 °C in air.

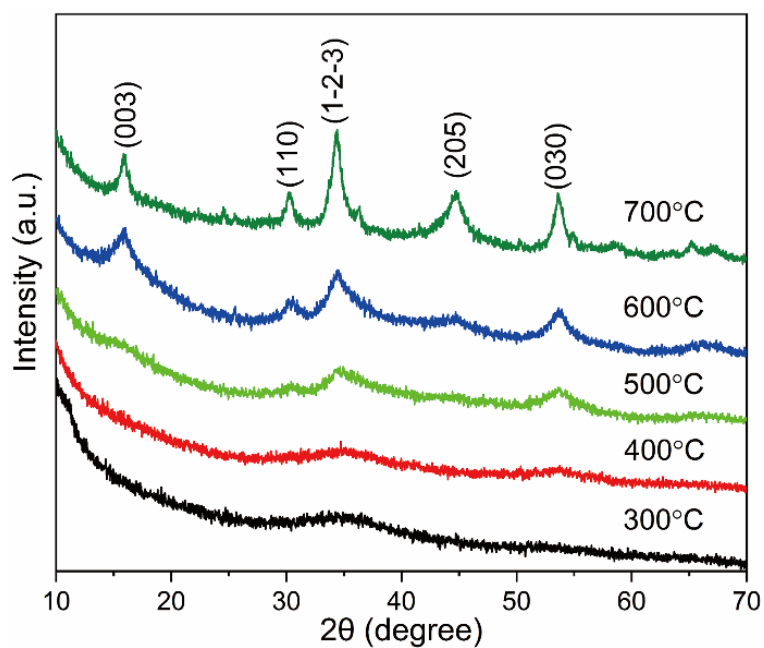


Figure S4. The XRD patterns for $[\text{Cr}_7\text{S}_8(\text{SCN})_4(\text{NH}_3)_{14}](\text{SH})$ after being heated at low level vacuum condition. The $\text{Cr}_2\text{S}_{3-x}\text{O}_x$ emerges at 500 °C.

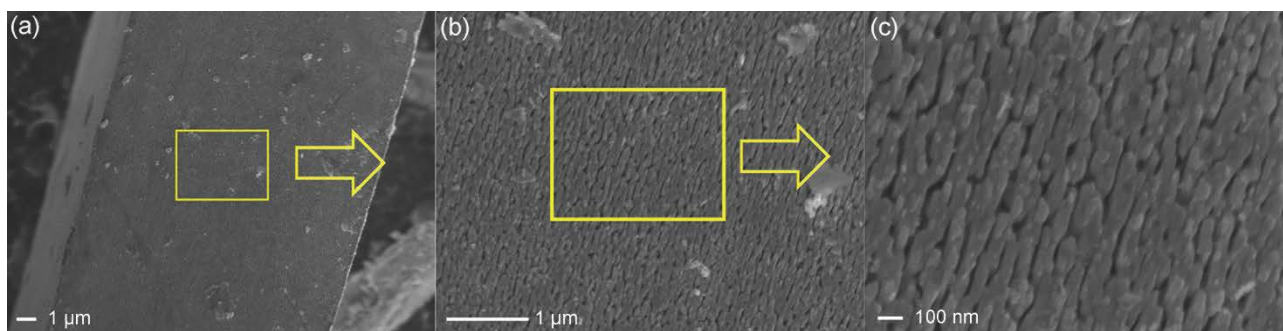


Figure S5. SEM images of the thermal resultant ($\text{Cr}_2\text{S}_{3-x}\text{O}_x$) for $[\text{Cr}_7\text{S}_8(\text{SCN})_4(\text{NH}_3)_{14}](\text{SH})$ heated at $500\text{ }^\circ\text{C}$.

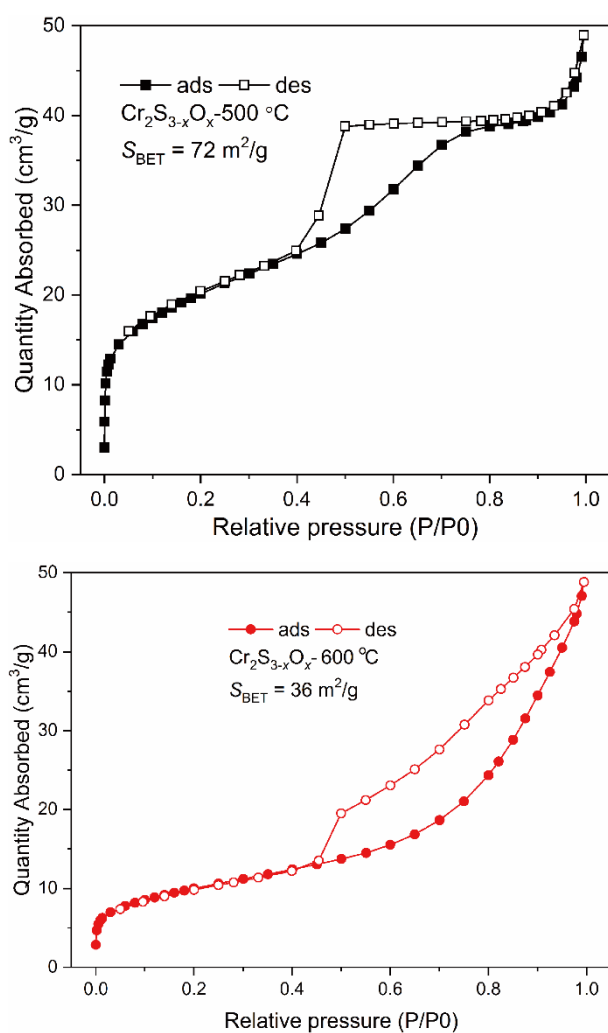


Figure S6. N_2 adsorption-desorption isotherms at 77 K for $\text{Cr}_2\text{S}_{3-x}\text{O}_x$ after being heated at 500 and 600 $^\circ\text{C}$. The calculated surface areas are given in the pattern.

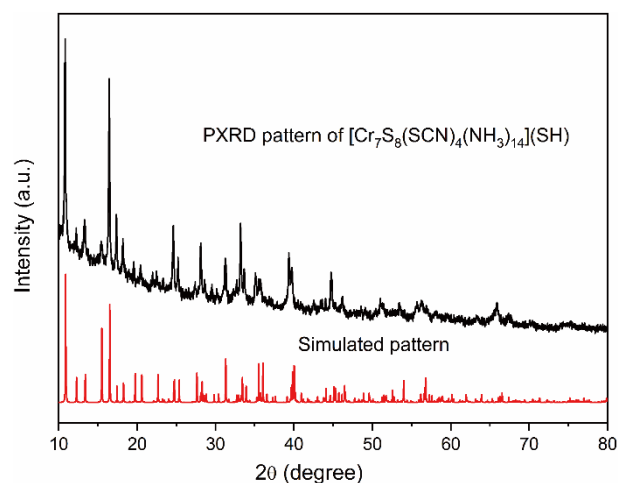


Figure S7. The experimental (black) and simulated (red) powder X-ray diffraction (PXRD) patterns for $[\text{Cr}_7\text{S}_8(\text{SCN})_4(\text{NH}_3)_{14}](\text{SH})$. The observed discrepancy in intensity between the experimental and calculated PXRD patterns is ascribed to the preference orientation of the powdered samples, which were not well grinded before PXRD data collection. The cell parameters from powder and single XRD also have a slight difference, which will lead to the mismatch in 2θ .